Analysis and Experimental Study of Gas Penetration in a Gas-Assisted Injection-Molded Spiral Tube

S. C. CHEN,* K. F. HSU, and K. S. HSU

Mechanical Engineering Department, Chung Yuan University, Chung-Li, Taiwan 32023, Republic of China

SYNOPSIS

Characteristics of gas penetration and polymer melt flow in gas-assisted injection molded spiral tubes was investigated by simulations and experiments. Distribution of the skin melt thickness along the gas flow direction was measured, and gas penetration in the primary and secondary stages was identified. An algorithm based on the control-volume/finite-element method combined with a particle-tracing scheme using a dual-filling-parameter technique is utilized to predict the advancements of both melt front and gas front during the molding process. The simulated distribution of gas penetration shows reasonably good coincidence with experimental observations. © 1995 John Wiley & Sons, Inc.

INTRODUCTION

Gas-assisted injection molding is one of the innovative multicomponent injection molding processes recently developed. In gas-assisted injection molding, the mold cavity is partially filled with polymer melt followed by the injection of inert gas into the core of the polymer melt.[1,2] A schematic diagram of gas-assisted injection molding is illustrated in Figure 1. Despite the advantages associated with the process, additional gas-related process parameters are introduced. Part design using thick ribs as gas channels to guide gas flow to the desired location is also critical to the successful application of the process. Due to the complexity of gas channel design, process control, as well as different flow characteristics between the gas and melt, computer simulation is expected to become an important required tool to help for both part design and process evaluation in the coming age. Nearly a decade ago, a simulation model based on the Hele–Shaw type of flow was developed to describe the polymer melt flow in thin cavities during conventional injection molding. These simulations provide acceptable predictions from the engineering application viewpoint. The existing models meet the new challenge and must be adopted to handle both gas and melt flows in the cavities of nonuniform thickness. A numerical algorithm for the simulation of gas and melt front advancements as well as an empirical model describing coating melt layer existing between the solidified melt and gas/melt interface (Fig. 2) as a function of processing parameters and material properties, are required for an accurate simulation. Fundamental studies on the characteristics of gas flow within the viscous melt are still lacking. A recent study concerning bubble penetration within viscous silicone paste in a tube under isothermal condition was reported by Poslinski and Stokes.[3] That investigation ended up with a prediction that a high gas pressure will result in longer gas penetration length. This is contrary to many experimental observations, e.g., in Barton and Turng[4] and Chen et al.[5] In addition, the experimental set-up is not only far away from actual molding conditions, but also does not consider secondary gas penetration resulting from melt shrinkage. In the present article a spiral-tube mold was designed to provide a preliminary investigation on the characteristics of gas penetration in the gas-assisted molding process. Gas and polymer melt flows in the spiral tube are basically one-dimensional. Formation and thickness of the coating melt layer between the solidified melt and gas were studied and measured from experiments. To find a numerical scheme suitable for the calculation of both melt and gas front advancements, an algorithm based on the control-vol-

* To whom correspondence should be addressed.

Journal of Applied Polymer Science, Vol. 58, 793–799 (1995)
 CCC 0021-8995/95/040793-07

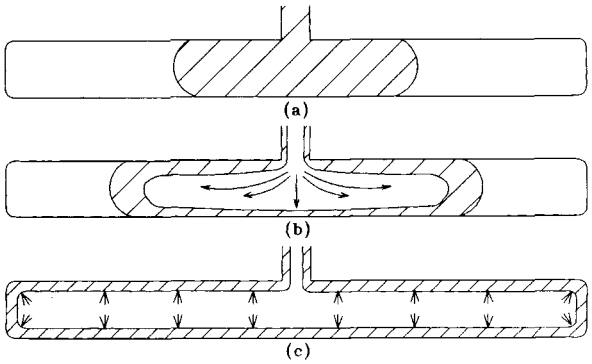

Figure 1 Schematic of gas-assisted injection-molding process: (a) partial melt filling of cavity; (b) gas is injected to complete melt filling; (c) gas continues to exert pressure during postfilling stage.

ume/finite-element approach combined with a newly developed particle-tracing scheme was employed. The present scheme is modified from that used for two-materials front advancements in the coinjection molding process reported recently.[6] Simulated results for gas and polymer melt front advancements are compared with experimental observations.

MODELING AND FORMULATION

Within the melt filled region, the relevant governing equations for the inelastic, non-Newtonian melt flow under nonisothermal conditions in a tube of circular cross section are based on the Hele–Shaw flow model and are written in cylindrical coordinates by:

$$\frac{\partial}{\partial z}(\pi R^2 \bar{w}) = 0 \tag{1}$$

$$\frac{\partial P}{\partial z} = \frac{1}{r}\frac{\partial}{\partial r}\left[r\left(\eta\frac{\partial w}{\partial r}\right)\right] \tag{2}$$

$$\rho C_p\left(\frac{\partial T}{\partial t} + w\frac{\partial T}{\partial z}\right) = \left[\frac{1}{r}\frac{\partial}{\partial r}\left(rk\frac{\partial T}{\partial r}\right)\right] + \eta\left(\frac{\partial w}{\partial r}\right)^2 \tag{3}$$

where P and T represent pressure and temperature; w is the velocity in the axial direction, z; r is the radial direction; $\bar{w}$ is the averaged velocity of w along the radial direction; and R is the radius of the runner. Equations (7) and (8) can also be formulated into an integrated form described by

$$\frac{\partial}{\partial z}\left(\pi S\frac{\partial P}{\partial z}\right) = 0 \tag{4}$$

with

$$S = \int_0^R \frac{r^3}{2\eta}\,dr. \tag{5}$$

In addition, η, ρ, C_p, and k are viscosity, density, specific heat, and thermal conductivity for the polymer melt, respectively. Viscosity of the polymer melt is described by a form of modified Cross model with Arrhenius temperature dependence, that is,

$$\eta(T, \dot{\gamma}) = \frac{\eta_0(T)}{1 + (\eta_0\dot{\gamma}/\tau^*)^{1-n}}$$

$$\text{and} \quad \eta_0(T) = B\exp\left(\frac{T_b}{T}\right). \tag{6a,b}$$

During the gas injection stage, gas within the gas filled region is assumed to be of uniform pressure. Coating melt thickness distribution under a specified molding condition is determined from the experiments. Therefore, formulation for the physical and mathematical models describing the gas/melt interface can be avoided at the present stage.

During the packing and cooling stages, gas continues to penetrate as a result of melt shrinkage. Calculation of melt shrinkage is based on the $P - V - T$ equation of state proposed by Tait[9] in the form of

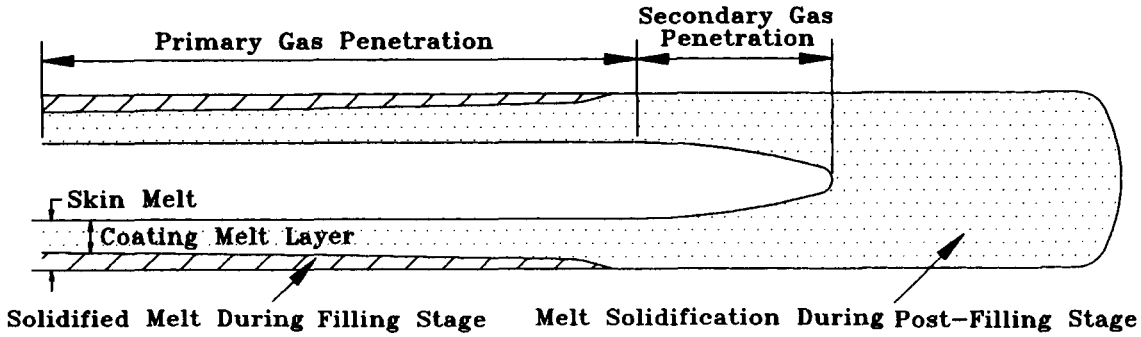

Figure 2 Schematic of coating melt layer formation between gas/melt interface and solidified melt during gas penetration.

$$\frac{V_o(T) - V(T,P)}{V_o(T)} = C \ln\left(1 + \frac{P}{b(T)}\right) \quad (7)$$

where $b(T) = b_1 \exp(-b_2 T)$, $V_o(T) = V_g + b_3(T - T_g)$; $C = 0.0894$ (university constant); and V, and T_g are specific volume and glass transition temperature of the polymer melt, respectively.

NUMERICAL ALGORITHM

Algorithm for Melt Front Advancement During Melt Injection

In solving the pressure field during melt injection, the control-volume/finite-element approach used for conventional injection molding by Wang et al.[7] and Chen et al.[8] is employed directly. The net flow, $q_i^{(l)}$, that enters its control volume, centered at node A (Fig. 3), from an adjacent element l can be represented by

$$q_i^{(l)} = S^{(l)} \cdot \sum_{k=1}^{2} \cdot D_k^{(l)} \cdot P_k^{(l)} \quad (8)$$

where i is the local index for node A in element l and $i = 1$ or 2 for rodlike elements. Subscript k denotes the local node index in element l and $D_{ik}^{(l)}$ is the influence coefficient of the nodal pressure to the net flow in element l. Linear interpolation function is used for rod elements. Values of $D_{ik}^{(l)}$ are equal to

$$D_{ik}^{(l)} = (-1)^{i+k} \frac{\pi}{2L^{(l)}} \quad (9)$$

where $L^{(l)}$ is the length of the rod element. At the entrance, the net flows from all adjacent elements must satisfy the following relation:

$$\sum_{l'} q_i^{l'} = \frac{Q}{2} \quad (10)$$

where Q is the total volumetric flow rate of the polymer melt. For the interior nodes, the net flows from all adjacent elements obey the conservation law of mass and are equal to zero, i.e.,

$$\sum_{l'} q_i^{l'} = 0. \quad (11)$$

Equations (10) and (11) can be finally integrated and assembled into a matrix form of

$$[K]\{P\} = \{G\} \quad (12)$$

where $[K]$ is the element coefficient matrix; $\{P\}$ is the column matrix associated with pressure, P; and $\{G\}$ is the column matrix for variable, $G_m \cdot G_m = Q/2$ if m, represented in a global node index number, is the entrance node of polymer melt. Otherwise, $G_m = 0$. To trace melt front advancement, a filling parameter, f_{melt}, is introduced to distinguish the entrance node and the interior nodes from the melt front nodes. f_{melt} is equal to 1 for entrance node and interior nodes whereas $0 < f_{\text{melt}} < 1$ for melt front nodes. When f_{melt} is 0, the node is designated as an empty node. A schematic diagram of node definition is shown in Figure 4(a). Once the pressure field is solved, radial velocity profile and the associated shear rate values can be calculated. At the melt fronts, a uniform profile for temperature and radial-averaged velocity is assumed to count for the fountain flow effect. In solving the temperature field, the same method reported previously is used.[7,8]

Algorithm for Gas and Melt Front Advancements During Gas Injection

Once the gas was injected into the mold, the domain filled with gas is assumed to be of uniform pressure. Pressure at the gas front is assumed to be the injected gas pressure and the total flow rate of the melt is treated as unknown. Once the melt flow rate is solved, gas flow rate and the associated gas front advancement are determined and the filling parameter is updated. To calculate the gas front advance-

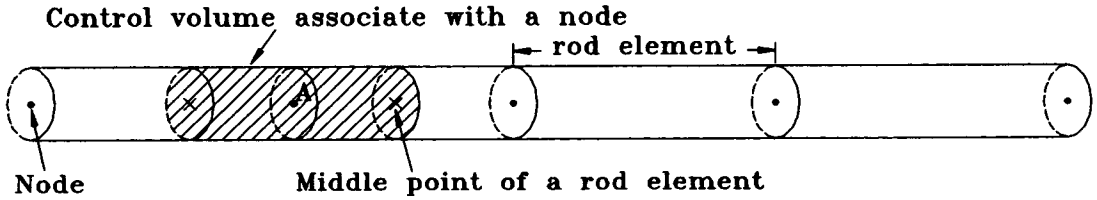

Figure 3 Schematic of control volume for a circular tube represented by a two-node rod element.

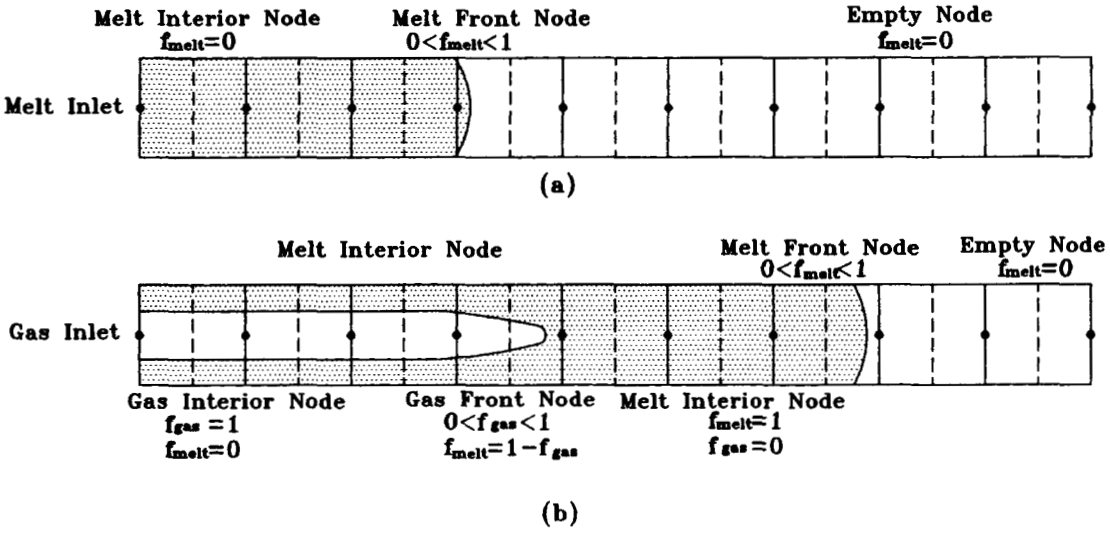

Figure 4 (a) Melt filling parameter defined for node identification during melt injection period. (b) Gas filling parameter defined for node identification during gas injection period.

ment it is necessary to introduce the second filling parameter, f_{gas}, to identify gas front nodes and gas interior nodes in each analysis interval as specified in Figure 4(b). The algorithm is similar to our particle-tracing algorithm developed for skin and core melt front advancements in coinjection molding reported recently.[6]

During the postfilling process, the polymer melt shrinks and gas continues to flow resulting in "secondary gas penetration." Calculation of secondary penetration for the gas is based on the temperature profile and the $P - V - T$ equation on each grid layer along the radial direction.

EXPERIMENTAL

A 75 ton Battenfeld 750/750 coinjection molding machine and an airmold system were used for the present experiments. Melt temperatures for polystyrene (PS) resin are 230°C. Mold temperature is 60°C. The spiral part of the uniform circular cross

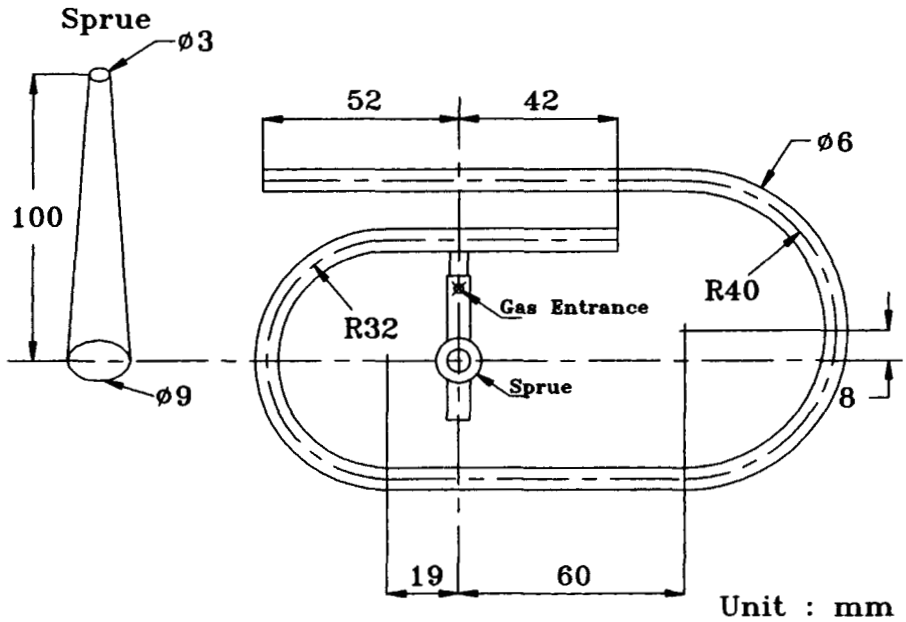

Figure 5 Mold geometry of the spiral tube.

section as shown in Figure 5 was designed to conduct the experimental studies. The diameter of the spiral tube is 0.006 m. Gas was injected after 84% of full injection shot (0.55 s) at a pressure of 140 bar. Distribution of coating melt layer thickness was investigated.

For PS (CHI MEI/PG33) materials constants in the modified Cross model used for viscosity values are n = 0.2838, τ^* = 1.791E + 04 Pa, B = 2.591E − 07 Pa · s, and T_b = 11680 K. Density, specific heat, and thermal conductivity of PS are 940 kg/m^3, 2100 J/kg · K and 0.18 W/m · K, respectively. Constants in the Tait $P - V - T$ equation can be found elsewhere.[9]

RESULTS AND DISCUSSION

One typical gas-assisted injection-molded spiral tube is shown in Figure 6. It was found that the skin melt thickness is rather uniformly distributed behind the gas front. Around the gas front, secondary gas penetration resulting from melt shrinkage was also observed. One of the results is shown in Figure 7. Detailed experimental results were analyzed and described by Chen et al.[5] The measured coating melt thickness ratio in the primary gas penetration period was about 0.36. Using this measured ratio, simulated results for the gas front advancement at different stages of primary gas penetration period are shown in Figure 8. Experimental observation of the gas front location (26 cm) is also indicated. Simulated result (26.3 cm) shows reasonably good consistency with the experimental observation. The secondary gas penetration during the postfilling phase was also estimated using radial temperature profile and the $P - V - T$ equation of state. The predicted location (34.5 cm), although slightly underestimated, was also consistent with the observed location (36 cm). This indicates that the present numerical algorithm provides good methodology for the simulation of gas and melt front advancements during gas-assisted injection molding in a one-dimensional flow geometry. Moreover, the concept of the algorithm can be extended and applied to the three-dimensional thin part laid out with gas channels of circular cross section.[5] However, processing effects on the coating layer ratio remain to be investigated from a variety of experiments such that coating melt thickness does not have to be known as *a priori* during simulation.

CONCLUSIONS

A numerical algorithm based on the control-volume/finite-element method combined with the particle tracing scheme suitable for two-component flow was developed to simulate gas and melt front advancements during the gas-assisted injection-molding process. Simulated results are also compared with

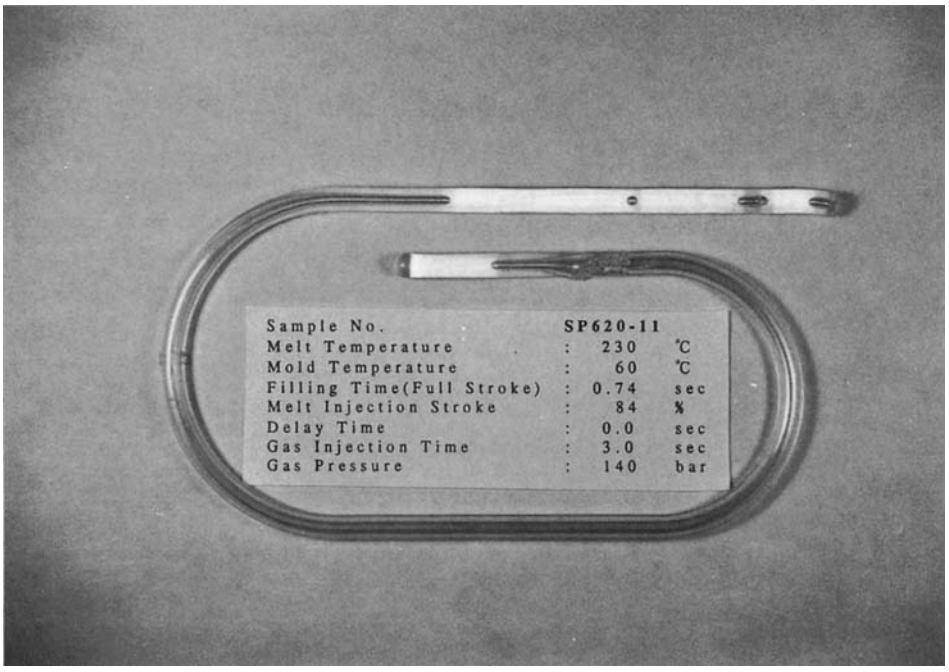

Figure 6 Gas-assisted injection-molded spiral tube.

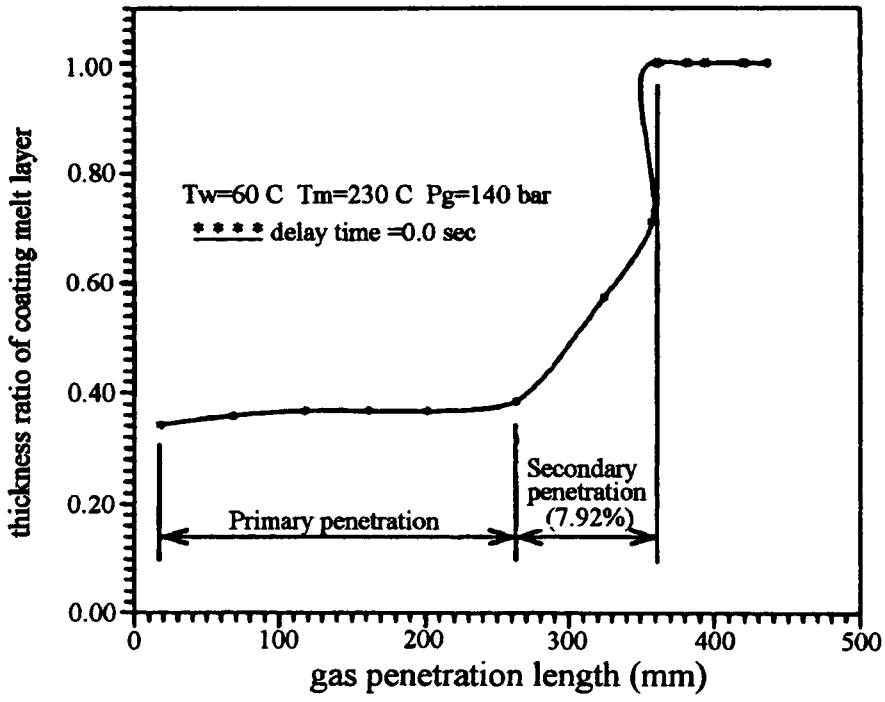

Figure 7 Distribution of skin melt thickness ratio along the tube at 140 bar gas injection pressure.

experimental observation. Although the effects of the processing condition on the coating layer ratio remain to be investigated to establish a general empirical formula, the current numerical scheme provides reasonably good results in the prediction of gas penetration.

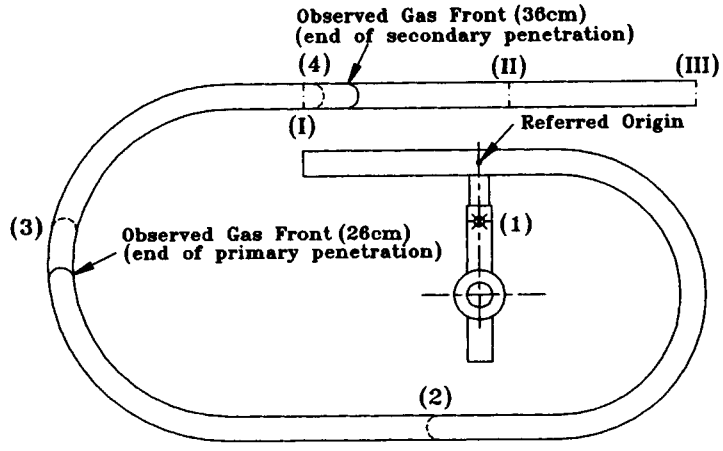

Simulation Results of Gas and Melt Front Locations:

(1),(I) gas and melt fronts at beginning of gas injection
(2),(II) gas and melt fronts after 0.075 seconds of gas injection
(3),(III) gas and melt fronts after 0.09 seconds of gas injection
(4) gas front at end of secondary penetration

Figure 8 Predicted and experimental results of gas front locations during primary and secondary gas penetration.

NOMENCLATURE

B	viscosity constant, Eq. (6b)
C_p	specific heat of polymer melt
k	thermal conductivity of polymer melt
n	viscosity constant, Eq. (6a)
P	pressure
R	radius of tube
r	radial direction of tube
S	fluidity, Eq. (5)
T	emperature
T_b	reference temperature, Eq. (6b)
V	specific volume of polymer melt
w	velocity in axial direction of tube
$\bar{w}$	averaged velocity along r direction for w
z	axial direction of tube
η	viscosity
η_0	viscosity constant, Eq. (6a)
$\dot{\gamma}$	shear rate, Eq. (6a)
ρ	density of polymer melt
τ^*	viscosity constant, Eq. (6b)

REFERENCES

1. K. C. Rush, *Plast. Eng.*, **July,** 35 (1989).
2. S. Shah, *SPE Tech. Paper,* **37,** 1494 (1991).
3. A. J. Poslinski and V. K. Stokes, *SPE Tech. Paper,* **39,** 68 (1993).
4. B. S. Barton and L. S. Turng, *SPE Tech. Paper,* **38,** 452 (1994).
5. S. C. Chen, M. C. Jeng, K. F. Hsu, and K. S. Hsu, *Prog. Rept.,* NSC (1994).
6. S. C. Chen and K. F. Hsu, to appear in Numerical Heat Transfer, Part A, **38**(5) (1994).
7. V. W. Wang, C. A. Hieber, and K. K. Wang, *J. Polym. Eng.*, **7,** 21 (1986).
8. S. C. Chen, P. Pai, and C. Hsu, *SPE Tech. Paper,* **34,** 250 (1988).
9. V. W. Wang and C. A. Hieber, *SPE Tech. Paper,* **34,** 290 (1988).

Received September 23, 1994
Accepted April 24, 1995